Supplementary Information

1 Dynamics of the Tb 4-level system

1.1 Wave functions of the crystal field levels

The point group of the Tb ions within the pyrochlore lattice is C_3. We refer to the 3-fold rotation axis as the local z-axis. This symmetry implies that J_z modulo 3 ($J_z mod 3$) is a good quantum number, that is, the crystal field levels within the ground state multiplet are superpositions of levels with values J_z whose differences are multiples of 3. Non-degenerate CF levels are formed by the eigenstates with $J_z mod 3 = 0$. The eigenstates with $J_z mod 3 = 1,2$ form symmetry protected multiplets with their time reversed counterparts (taking values of J_z mod 3 with opposite sign). The two lowest-lying CF eigenstates of Tb in $Tb_2Ti_2O_7$ form two such doublets, which we denote by G (ground) and E (excited). We further refer to the states with fixed $J_z mod 3$ as $\uparrow/\downarrow$, according to the sign of the expectation value $\langle J_z \rangle$ of the magnetic moment along z.

The diagonalization of the CF Hamiltonian yields the explicit wavefunctions (using the shorthand notation $|m\rangle = |j = 6, m\rangle$) using the coefficients tabulated in table IX of reference [31].

$$|G\uparrow\rangle \quad = \quad a_1|4\rangle - b_1|1\rangle + c_1|-2\rangle + d_1|-5\rangle \qquad (1)$$
$$|G\downarrow\rangle \quad = \quad T|G\uparrow\rangle = a_1|-4\rangle + b_1|-1\rangle + c_1|2\rangle - d_1|5\rangle \qquad (2)$$

with $a_1 = 0.9116$, $b_1 = 0.1186$, $c_1 = 0.1765$, $d_1 = 03519$, whereby the time reversal operator acts as $T|m\rangle = (-1)^m|-m\rangle$. The magnetic moment of the ground state doublet is $m_G = \langle G\uparrow|J_z|G\uparrow\rangle = -\langle G\downarrow|J_z|G\downarrow\rangle = 2.657$.

For the excited doublet one finds

$$|E\uparrow\rangle \quad = \quad a_2|5\rangle - b_2|2\rangle + c_2|-1\rangle + d_2|-4\rangle \qquad (3)$$
$$|E\downarrow\rangle \quad = \quad T|E\uparrow\rangle = -a_2|-5\rangle - b_2|-2\rangle - c_2|1\rangle + d_2|4\rangle \qquad (4)$$

with $a_2 = 0.8910$, $b_2 = 0.2320$, $c_2 = 0.1085$, $d_2 = 0.3748$, having a larger magnetic moment $m_E = \langle E\uparrow|J_z|E\uparrow\rangle = -\langle E\downarrow|J_z|E\downarrow\rangle = 3.503$.

The energy difference between the two doublets is

$$\Delta E = E_E - E_G = 1.6\text{meV}. \qquad (5)$$

1.2 Matrix elements for the interaction with an applied magnetic field

Let us now study how an external magnetic field couples to this pair of doublets. The magnetic field acts via the interaction Hamiltonian $H_B(t) = -g_J\mu_B\vec{B}(t)\cdot\vec{J}$, where $g_J = 3/2$ is the Landé factor of the considered Tb$^7F_6$-multiplet and μ_B is the Bohr magneton. Even though we will discuss general pulses, it is useful to consider the limit of a harmonic driving field $g_J\mu_B\vec{B}(t) = \vec{\mathcal{B}}(t) = \mathcal{B}_0\vec{e}\exp(-i\omega t) + \text{H.c.}$, where $\mathcal{B}_0 = 1/2B_0$ is a real amplitude and $\vec{e}$ the polarization vector. For linearly polarized light $\vec{e}$ can be chosen to be real, while circularly polarized light is characterized by a complex $\vec{e}$ in general. For a general pulse shape, $\mathcal{B}_0 \to \mathcal{B}_0(t)$ is a smoothly varying envelope function.

The J^z operator only has matrix elements between states with equal value of $J_z mod 3$ (i.e., between $|G,\uparrow\rangle$ and $|E,\downarrow\rangle$, and between $|G,\downarrow\rangle$ and $|E,\uparrow\rangle$, while the operators $J_\pm = J_x \pm iJ_y$ are purely off-diagonal in the basis of fixed $J_z mod 3$. With the above wavefunctions one finds the following non-zero (real) matrix elements between ground and excited doublets

$$j_z \quad \equiv \quad \langle E,\downarrow|J_z|G,\uparrow\rangle = -\langle E,\uparrow|J_z|G,\downarrow\rangle = 3.029, \qquad (6)$$
$$j_\perp \quad \equiv \quad \frac{1}{2}\langle E,\uparrow|J_+|G,\uparrow\rangle = -\frac{1}{2}\langle E,\downarrow|J_-|G,\downarrow\rangle = 2.362. \qquad (7)$$

The action of a magnetic field in this pair of doublets is best understood within a rotating wave approximation (RWA). The latter is justified for driving close to the resonance frequency, $\omega \approx \Delta E/\hbar$ and at moderate driving strength ($j_{z,\perp}\mathcal{B}_0 \ll \Delta E = 1.6 meV$), where non-resonant intra-doublet and fast-oscillating inter-doublet couplings can safely be neglected. These conditions are met only approximately by our experimental parameters: the central frequency of the driving pulse is $\hbar\omega = 2.4\, meV$ and $j_{z,\perp}\mathcal{B}_0 = j_{z,\perp}\, g_J\mu_B B_{0,p}/2 \approx 0.03\, meV$ using the experimentally determined magnetic field peak amplitude of $B_{0,p}$ = 0.25T and approximating $j_{z,\perp}$ with a typical value of 3. However, the approximation still gives useful insight into the main effect of the driving. Within the RWA the resulting driving Hamiltonian then reduces to

$$H_B(t) \to H_{RWA}(t) = -\mathcal{B}_0 e^{-i\omega t} \sum_{\alpha,\beta\in\{\uparrow\downarrow\}} M_{\alpha\beta}|E,\alpha\rangle\langle G,\beta| + H.c., \quad (8)$$

where the 2x2 matrix $M_{\alpha\beta}$ is given by

$$M = \sum_{a=x,y,z} e_a \hat{J}_a^{EG} \qquad (9)$$

with the inter-doublet matrix elements of the magnetic moment operators given by

$$\begin{aligned} \hat{J}_x^{EG} &= j_\perp \sigma^z, \\ \hat{J}_y^{EG} &= -ij_\perp, \quad (10) \\ \hat{J}_z^{EG} &= -ij_z\sigma^y. \end{aligned}$$

where the $\sigma^{x,y,z}$ are the standard Pauli matrices.

1.3 Temporal evolution in the rotating frame

We seek the solution to the time-dependent Schrödinger equation $i\partial_t\psi = [H_{CF} + H_{RWA}(t)]\psi$ in the form

$$\psi(t) = \sum_\alpha [e_\alpha(t)|E,\alpha\rangle e^{-iE_E t} + g_\alpha(t)|G,\alpha\rangle e^{-iE_G t}] \qquad (11)$$

where at the level of the RWA and for resonant driving $\omega = \Delta E/\hbar$, the coefficients e_α, g_α obey the Schrödinger equation in the rotating frame,

$$\begin{aligned} i\partial_t e_\alpha(t) &= -\mathcal{B}_0 \sum_\beta M_{\alpha\beta} g_\beta(t)\,, \\ i\partial_t g_\alpha(t) &= -\mathcal{B}_0 \sum_\beta M_{\alpha\beta}^\dagger e_\beta(t)\,. \qquad (12) \end{aligned}$$

Taking a second derivative, one finds a closed differential equation for the ground state amplitude vector $g = \binom{g_\uparrow}{g_\downarrow}$ alone,

$$-\partial_t^2 g(t) = \mathcal{B}_0^2 M^\dagger M g(t), \qquad (13)$$

using matrix notation.

1.4 Splitting of the four-level systems into effective two-level systems

The Hermitian matrix $M^\dagger M$ is positive definite and diagonalizable. We call $\phi_{1,2}$ its orthonormal eigenvectors, and $d_{1,2}^2$ the corresponding eigenvalues. The explicit form of the matrix $M^\dagger M$ is

$$M^\dagger M = A + \vec{v}\cdot\vec{\sigma}, \quad (14)$$

where

$$\begin{aligned} A &= |\vec{b}|^2, \\ v_x &= -2Re(b_z^* b_x), \\ v_y &= 2Re(b_z^* b_y), \\ v_z &= 2Im(b_x^* b_y), \quad (15) \end{aligned}$$

and we have used the notation $b_z \equiv e_z j_z$, $b_{x,y} \equiv e_{x,y} j_\perp$. From this, one finds that $\phi_{1,2}$ are the eigenvectors of $\vec{v}\cdot\vec{\sigma}$ with eigenvalue $\pm|\vec{v}|$. The associated magnetic moments are, respectively,

$$d_{1,2} = \sqrt{A \pm |\vec{v}|}. \qquad (16)$$

For linear polarization, the b_α are real, and the magnetic moments evaluate to

$$d_{1,2} = ||b_z| \pm |b_\perp|| = ||e_z j_z| \pm |e_\perp j_\perp||, \qquad (17)$$

with $b_\perp = \sqrt{b_x^2 + b_y^2}$, and $e_\perp = \sqrt{e_x^2 + e_y^2}$.

Note that ϕ_i only couples to one excited state, ψ_i. Therefore, $\{\phi_1, \psi_1\}$ and $\{\phi_2, \psi_2\}$ form two independent effective two-level systems. The ψ_i span an orthonormal basis of the excited doublet space, being the eigenvectors of $MM^\dagger$, for which one finds

$$MM^\dagger \quad = \quad \sigma^x(A - \vec{v} \cdot \vec{\sigma})\sigma^x. \quad (18)$$

Up to phases its eigenvectors are thus $\psi_{1,2} \propto \sigma^x \phi_{2,1}$.

1.5 Driven dynamics of the effective two-level systems

In the basis $\{\phi_i, \psi_i\}$, the full driving Hamiltonian takes the form

$$H_{res} = \begin{pmatrix} 0 & -\mathcal{B}(t)d_1 & 0 & 0 \\ -\mathcal{B}(t)d_1 & \Delta E & 0 & 0 \\ 0 & 0 & 0 & -\mathcal{B}(t)d_2 \\ 0 & 0 & -\mathcal{B}(t)d_2 & \Delta E \end{pmatrix}, \quad (19)$$

where we dropped the non-resonant intra doublet couplings. d_i can be seen as the effective magnetic moment of the two-level systems and $\Omega_{R,i} = \mathcal{B}_0 d_i/\hbar$ is the associated instantaneous Rabi frequency. The 2×2 Hamiltonian governing the effective TLS generates the unitary, non-dissipative part of the dynamics for the ensemble averaged density matrix $\rho = \overline{|\psi(t)\rangle\langle\psi(t)|}$, $\partial_t \rho = -i/\hbar[H_{res}, \rho]$ of Eqs. (3, 4) in the main text. Defining the resonance frequency $\omega_0 = \Delta E/\hbar$ and the occupation difference $\Delta n(t) = \rho_{00}(t) - \rho_{11}(t)$, we obtain:

$$\frac{d\Delta n(t)}{dt} = \frac{2id\mathcal{B}(t)}{\hbar}\left(\rho_{10}(t) - \rho_{10}^*(t)\right); \quad (20)$$

$$\frac{d\rho_{10}(t)}{dt} = -i\omega_0\rho_{10}(t) + i\frac{d\mathcal{B}(t)}{\hbar}\Delta n(t). \quad (21)$$

Recalling that $\mathcal{B}(t) = g_J \mu_B B(t)$ yields the non-dissipative part of equations (3-4) of the main text, where $|\mathrm{d}| \approx j_{typ} = 3$ interpolates between the transverse and longitudinal transition matrix elements, $j_\perp, j_z$.

Given the modest excitation level, one may approximate $\Delta n(t)$ in (22) by Δn_{eq}, which yields the coherence:

$$\rho_{10}(t) = \frac{i}{\hbar}\Delta n_{eq} d \int_{-\infty}^{t} dt' \; \mathcal{B}(t')\, \mathrm{e}^{\left(-i\omega_0 - \frac{1}{\tau_c}\right)(t-t')}, \quad (22)$$

which is proportional to the occupation difference before excitation Δn_{eq}.

Note that in the low temperature state (below the Curie-Weiss temperature $|\Theta_{CW}| = 13\ K$), the interactions induce correlations and entanglement among the different Tb ions. However, since we focus on relatively short times as compared to the inverse interaction strength and since we consider only a moderate level of excitation, we neglect those correlations and describe the driving at the level of the single site density matrix. In the main text, the interaction with neighboring sites are summarily accounted for by including a relaxation and dephasing rate (of the order of the Tb-Tb interaction strength) in the evolution equation for the single site density matrix.

1.6 Unitary dynamics within RWA approximation

We now return to the RWA ansatz (11), where only the resonant frequency component at $\omega = \pm\omega_0$ of $\mathcal{B}(t)$ is retained. In a thermal ensemble at temperature $k_B T \ll \hbar\omega_0$, the initial wavefunction $\psi(0)$ restricted to a given Tb site is a random state within the ground doublet, $e_\alpha(t = -\infty) = 0$. Within the RWA the general solution of the resonantly driven Schrödinger equation reads

$$\begin{aligned} g(t) &= C_1 \cos\left(d_1 F(t)\right)\phi_1 + C_2 \cos\left(d_2 F(t)\right)\phi_2, \\ e(t) &= iC_1 \sin\left(d_1 F(t)\right)\psi_1 + iC_2 \sin\left(d_2 F(t)\right)\psi_2, \end{aligned} \quad (23)$$

where

$$F(t) = \int_{-\infty}^{t} dt' \mathcal{B}_0(t') \, .$$

Observables pertaining to the subensemble of Tb ions with equally oriented local z-axis have to be averaged with the prescription $\overline{C_i^* C_j} = \delta_{ij} \, / \, 2$, and $\overline{C_i C_j} = 0$.

1.7 Time-evolving magnetization

The time-evolving magnetic moment of the Tb wavefunction is obtained as

$$\begin{aligned} m_\alpha(t) &= g_J \mu_B \langle \psi(t) | J_\alpha | \psi(t) \rangle \\ &= g_J \mu_B \delta_{\alpha,z} [m_G g^\dagger(t) \sigma^z g(t) + m_E e^\dagger(t) \sigma^z e(t)] \\ &\quad + 2 g_J \mu_B Re[e^{i\omega_0 t} e^\dagger(t) \hat{\mathrm{J}}_\alpha^{EG} g(t)]. \end{aligned} \tag{24}$$

Note that once the driving field is switched off, the wavefunctions in the rotating frame, $e(t), g(t)$ do not evolve further and would stay constant in the absence of interactions with other degrees of freedom. The first line in (24) captures the static, time-independent magnetization induced by the driving pulse $\mathcal{B}(t)$, while the second contribution to the magnetization oscillates with the frequency ω_0 and reflects the coherence of the wavefunction, being a superposition of components in the excited and ground state doublet. Interactions with neighboring Tb ions eventually induce dephasing, which degrades the oscillatory term, and relaxation, which makes the static part of the induced magnetization decay.

1.8 Oscillatory magnetization induced by linearly polarized light

For linearly polarized light the static part of the magnetization vanishes since the magnetic moments of the light-selected TLS vanish, $\langle \phi_i | J^z | \phi_i \rangle \sim \langle \phi_i | \sigma^z | \phi_i \rangle = \pm \frac{v_z}{|\vec{v}|} = 0$ and likewise for $\langle \psi_i | J^z | \psi_i \rangle$

The vector $\vec{v}$ in (15) is proportional to $(-e_x, e_y, 0)$. The eigenvectors associated to the effective magnetic moments $d_{1,2} = |b_\perp \mp b_z|$ are explicitly

$$\phi_{1,2} = \frac{1}{\sqrt{2}} \begin{pmatrix} \pm(e_x + i e_y) \, / \, e_\perp \\ 1 \end{pmatrix}, \tag{25}$$

and

$$\psi_{1,2} = sgn(b_\perp \mp b_z) \frac{1}{\sqrt{2}} \begin{pmatrix} \pm 1 \\ -(e_x + i e_y) \, / \, e_\perp \end{pmatrix}. \tag{26}$$

In this basis, the off-diagonal matrix elements of the magnetic moment operator $\hat{\mathrm{J}}^{EG}$ evaluate to

$$\psi_{1,2}^\dagger \begin{pmatrix} \hat{\mathrm{J}}_x^{EG} \\ \hat{\mathrm{J}}_y^{EG} \\ \hat{\mathrm{J}}_z^{EG} \end{pmatrix} \phi_{1,2} = sgn(b_\perp \mp b_z) \begin{pmatrix} j_\perp e_x \, / \, e_\perp \\ j_\perp e_y \, / \, e_\perp \\ \mp j_z \end{pmatrix}. \tag{27}$$

The oscillatory part of the magnetization results from Eq. (27) as

$$\begin{aligned} \overline{m_{x,y}^{osc}}(t) &= g_J \mu_B \overline{2 Re[e^{i\omega_0 t} e^\dagger(t) \hat{\mathrm{J}}_{x,y}^{EG} g(t)]} \\ &= g_J \mu_B \frac{j_\perp}{2} \frac{e_{x,y}}{e_\perp} \sin(\omega_0 t) \\ &\quad \times (\sin[2(j_\perp e_\perp + j_z e_z) F(t)] + \sin[2(j_\perp e_\perp - j_z e_z) F(t)]), \end{aligned} \tag{28}$$

and

$$\begin{aligned} \overline{m_z^{osc}}(t) &= g_J \mu_B \overline{2 Re[e^{i\omega_0 t} e^\dagger(t) \hat{\mathrm{J}}_z^{EG} g(t)]} \\ &= g_J \mu_B \frac{j_z}{2} \sin(\omega_0 t) \\ &\quad \times (\sin[2(j_\perp e_\perp + j_z e_z) F(t)] - \sin[2(j_\perp e_\perp - j_z e_z) F(t)]). \end{aligned} \tag{29}$$

To include dephasing, we switch to the density matrix formulation, approximating the subspaces of the two light-selected TLS $(\phi_i, \psi_i)_{i=1,2}$ as uncoupled. Let us discuss here the case of relatively weak or short pulses with $F_{max} \ll 1$, as used in the experiment. For the ensemble averaged magnetic moment one finds

$$\overline{m_\alpha(t)} = \frac{1}{2} g_J \mu_B \sum_{i=1,2} 2Re[(\psi_i^\dagger \hat{J}_\alpha^{EG} \phi_i)\rho_{01}^{(i)}], \qquad (30)$$

whereby the off-diagonal term of the density matrix of the TLS i, $\rho_{01}^{(i)}$, satisfies Eq. (21) with $d = d_i$. Resorting to the resonant approximation, writing $\vec{\mathcal{B}}(t) = \mathcal{B}_0 \vec{e} \exp(-i\omega_0 t) + \text{H.c.}$ and retaining only the positive frequency component, one finds the contributions of the two TLS to add up to yield

$$\begin{aligned} \overline{m_\alpha(t)} &= g_J \mu_B \sum_{i=1,2} (\psi_i^\dagger \hat{J}_\alpha^{EG} \phi_i) d_i \\ &\quad \times Re[i\exp(-i\omega_0 t) \int_{-\infty}^{t} dt' \mathcal{B}_0(t') e^{-(t-t')/\tau_c}] \\ &= 2 g_J \mu_B j_\alpha^2 e_\alpha \sin(\omega_0 t) \int_{-\infty}^{t} dt' \mathcal{B}_0(t') e^{-(t-t')/\tau_c}, \qquad (31) \end{aligned}$$

where we used the notation $j_x = j_y \equiv j_\perp$. Note that in this regime, where the excitation level remains modest, the time dependence of the contributions from the different TLS is the same, and is well captured by a single representative TLS, as was done in the main text.
For a weak pulse and upon neglecting dephasing (setting $\tau_c \to \infty$) this indeed coincides with the linearization of the results (28, 29),

$$\begin{aligned} \overline{m_{x,y}^{osc}}(t) &\approx e_{x,y}(g_J \mu_B j_\perp)^2 sin(\omega_0 t) \int_{-\infty}^{t} dt' B_0(t'), \\ \overline{m_z^{osc}}(t) &\approx e_z (g_J \mu_B j_z)^2 sin(\omega_0 t) \int_{-\infty}^{t} dt' B_0(t'), \qquad (32) \end{aligned}$$

where $B_0(t) = 2\mathcal{B}_0(t)/g_J\mu_B$ is the time-dependent linearly polarized magnetic field envelope of the pulse.

1.9 Inducing quasi-static magnetization by circularly polarized light

With circularly polarized pulses a quasi-static magnetization can be induced. Using the general solution (20) and (21), the ensemble average of the non-oscillatory magnetization (described by the first line in (24)) can be evaluated as

$$\begin{aligned} \overline{m_z^{stat}(t)}/g_J\mu_B &= \frac{m_G}{2}[\langle\phi_1|\sigma^z|\phi_1\rangle \cos^2(d_1 F(t)) + \langle\phi_2|\sigma^z|\phi_2\rangle \cos^2(d_2 F(t))] \\ &\quad + \frac{m_E}{2}[\langle\psi_1|\sigma^z|\psi_1\rangle \sin^2(d_1 F(t)) + \langle\psi_2|\sigma^z|\psi_2\rangle \sin^2(d_2 F(t))] \\ &= \frac{m_G - m_E}{2} \mu_z [\cos^2(d_1 F(t)) - \cos^2(d_2 F(t))], \qquad (33) \end{aligned}$$

where we used (19). This quasi-static magnetization settles to $F(t) \to F_{max}$ after the pulse.

As an example, we consider a CP pulse propagating along the local z-axis of one type of ions, with $B_y = iB_x \equiv iB$, $B_z = 0$. The matrix M takes the form $M = j_\perp B(\sigma^z + 1)$, from which one extracts $\phi_1 = (1,0)$, $d_1 = 2j_\perp = 4.724$; $\phi_2 = (0,1)$, $d_2 = 0$ and $\mu_z = 1$. This results in the induced static magnetization

$$\begin{aligned} \overline{m_z^{stat,\parallel}(t)}/g_J\mu_B &= \mu_z \frac{m_E - m_G}{2}(\cos^2(d_1 F(t)) - \cos^2(d_2 F(t))) \\ &= -\frac{m_E - m_G}{2} \sin^2(2 j_\perp F(t)) \\ &\approx 0.423 \sin^2(4.724 F(t)). \qquad (34) \end{aligned}$$

On average, half of these ions are in the state ϕ_1 which undergoes Rabi oscillations, a full population conversion leading to a change of magnetization by $m_E - m_G$

For the three differently oriented ions, one finds two non-trivial effective TLS, with effective magnetic moments $d_1' = 4.493$ and $d_2' = 2.919$, respectively, and magnetizations of the associated TLS basis vectors $\mu_z' \equiv \langle\phi_1|\sigma^z|\phi_1\rangle = -0.637$. Injecting this in the above formulae one finds the induced quasi-static magnetization along the ions' respective local z-axes to evaluate to

$$\overline{m_z^{stat,others}(t)}/g_J\mu_B \tag{35}$$

$$= \mu_z' \frac{m_G - m_E}{2}[\cos^2(d_1'F(t)) - \cos^2(d_2'F(t))]$$
$$= 0.2696(\cos^2(4.493F(t)) - \cos^2(2.919F(t))). \tag{36}$$

The moments of three different non-aligned ions sum up to a magnetization pointing along $-\vec{e}_z$, and having a magnitude $\overline{m_z^{stat,others}(t)}$.

In TTO a cell of volume $V = (10.3Å)^3\ /\ 4$ contains four Tb ions, one of each orientation, that we treat as uncorrelated. The total quasistatic magnetic moment induced in such a cell by a CP pulse of action F_{max}, oriented along the axis of one of the ions points along the propagation direction of the pulse and has a magnitude

$$m^{tot,stat}/g_J\mu_B = [0.423\sin^2(4.724F_{max}) \tag{37}$$
$$-0.2696(\cos^2(4.493F_{max}) - \cos^2(2.919F_{max}))].$$

For short/weak pulses, the final magnetic moment behaves as $m^{tot,slow}(t)/g_J\mu_B \approx 11.01F_{max}^2$. The average internal field resulting from this magnetization density follows as

$$B_{int} = \frac{2}{3}\mu_0\frac{m^{tot,stat}}{V}, \tag{38}$$

which can reach of the order of $20mT$ in $Tb_2Ti_2O_7$.
Due to interactions between the ions, the magnetization will, however, decay back to zero (thermal equilibrium) over a time scale of the order of τ via diffusion of the excitations. On the other hand the global excitation level (total energy) of the ions relaxes much more slowly, necessitating coupling to the phonon bath.

Supplementary Data

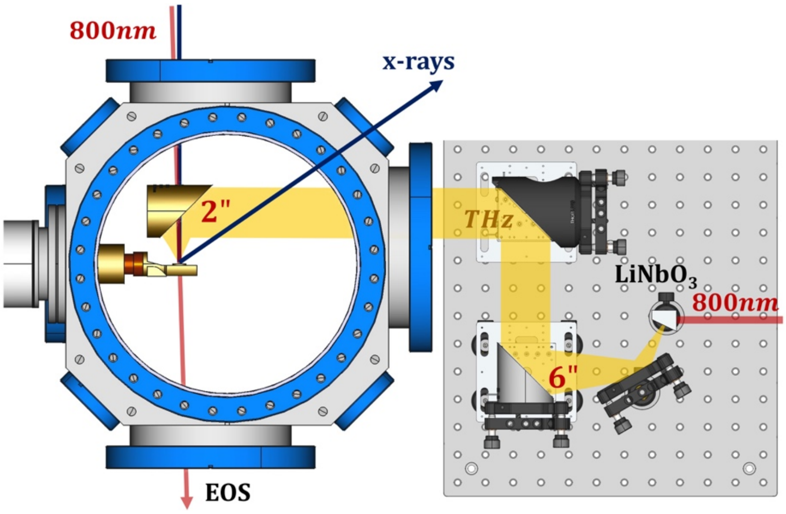

Supplementary Figure 1. Experimental geometry. The THz pulses (yellow) were generated outside the chamber and passed through a window into the vacuum chamber. They were focused with a 2" focal distance parabolic mirror in vacuum onto the sample and overlapped with the x-ray probe pulses (dark blue) on the sample. The THz electromagnetic field was characterized by electrooptic sampling (EOS) using 800nm pulses (red) outside the chamber. Part of this Figure has been reproduced from reference [42].

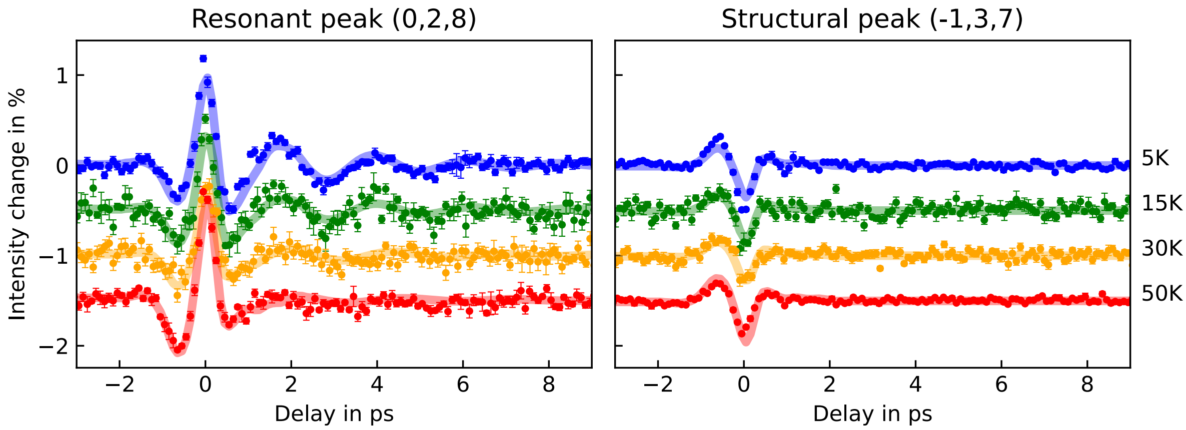

Supplementary Figure 2. Temperature dependence of the intensity change signal of the structural and resonant peaks. Intensity changes induced by the same THz excitation are shown at different temperatures for the resonant (028) peak (left side) and the structurally allowed (-137) peak.

Supplementary Table 1. Summary of the 4 unique Tb ion positions and local quantization axis, as well as the induced magnetic moment $\overrightarrow{\mathbf{m}_i}$ by the excitation on each site i with: $\boldsymbol{m}_{\perp,\boldsymbol{z}} = (\boldsymbol{g_J}\boldsymbol{\mu_B}\boldsymbol{j}_{\perp,\,z})^2\boldsymbol{sin}(\boldsymbol{\omega_0 t})\int_{-\infty}^{\boldsymbol{t}} \boldsymbol{dt'}\boldsymbol{B}(\boldsymbol{t'})\boldsymbol{e}^{-(\boldsymbol{t}-\boldsymbol{t'})/\boldsymbol{\tau_c}}$. The last column denotes their phase factors for the $(\boldsymbol{hkl}) = (\boldsymbol{028})$ peak.

Tb	Position *xyz*	$x_{local,i}$	$y_{local,i}$	$z_{local,i}$	Local magnetic moment $\overrightarrow{\mathrm{m}_i}$ on Tb site *i*	$\mathrm{e}^{2\pi i(hx+ky+lz)}$
1	(0, 0, 0)	[1 -1 0]	[1 1 -2]	[1 1 1]	$\left(\frac{m_\perp}{\sqrt{2}}, -\frac{m_\perp}{\sqrt{2}}, 0\right)$	1
2	(3/4, 1/4, 1/2)	[-1 1 0]	[-1 -1 -2]	[-1 -1 1]	$-\left(\frac{m_\perp}{\sqrt{2}}, -\frac{m_\perp}{\sqrt{2}}, 0\right)$	-1
3	(1/4, 1/2, 3/4)	[-1-1 0]	[-1 1 2]	[-1 1 -1]	$\left(-\frac{0.58m_\perp}{\sqrt{6}} - \frac{0.82m_z}{\sqrt{3}}, \frac{0.58m_\perp}{\sqrt{6}} + \frac{0.82m_z}{\sqrt{3}}, \frac{1.16m_\perp}{\sqrt{6}} - \frac{0.82m_z}{\sqrt{3}}\right)$	1
4	(1/2, 3/4, 1/4)	[1 1 0]	[1 -1 2]	[1 -1 -1]	$\left(\frac{0.58m_\perp}{\sqrt{6}} + \frac{0.82m_z}{\sqrt{3}}, -\frac{0.58m_\perp}{\sqrt{6}} - \frac{0.82m_z}{\sqrt{3}}, \frac{1.16m_\perp}{\sqrt{6}} - \frac{0.82m_z}{\sqrt{3}}\right)$	-1

Supplementary Table 2. Parameters used for the simulation of the time-dependent diffraction intensities of the structural ($\mathbf{\bar{1}37}$) and resonant ($\mathbf{028}$) Bragg peaks.

a_s in $\%/(MV/cm)$	$a_{s,o}$ in $\%/(MV/cm)$	a_m in $\%$	ν_0 in THz	τ_c in ps	τ in ps	Δn_{eq}
1.04 ± 0.08	-1.8 ± 0.1	17.4 ± 5.6	0.45 ± 0.02	2.4 ± 0.4	≈ 4	1